Clim Dyn (2010) 34:47–59
DOI 10.1007/s00382-009-0649-x

# Numerical simulation of seasonal distribution of precipitation over the eastern Mediterranean with a RCM

**Simon O. Krichak · Pinhas Alpert · Pavel Kunin**

Received: 6 July 2008 / Accepted: 7 August 2009 / Published online: 22 August 2009


**Abstract** Regional climate model (RCM) RegCM3 with 50 km horizontal resolution driven from the lateral boundaries by the data from NCEP/NCAR re-analysis is used in a series of ten climate downscaling experiments over the eastern Mediterranean (EM) region. Results of the experiments are characterized by seasonal precipitation patterns with notable offshore precipitation zones positioned ~50 km westward of a less intense precipitation zone over the coastal area. Atmospheric processes determining the distribution of seasonal precipitation patterns in the EM are analyzed based on results of the RCM experiments performed. Level of success of the model representation of the actual precipitation over the ECM appears to be depending on that of precipitation balance over different parts of the domain. Excessive moisture convergence over a sub-area usually takes place at the expense of moisture divergence from neighboring areas. Synoptic mechanism causing formation of the precipitation zone in the offshore zone appears to be associated with the role of meridionally oriented atmospheric trough systems extending from Scandinavia or Siberia to the EM during the period with rainy events. In such situations, air flows with strong northern components lead to intense transport of cold air masses to the EM. Meeting of the cold air masses the warm and humid air over the sea surface in the offshore zone causes formation of persistent squall lines and heavy rains there. Such processes may continue quite long as long as the troughs are stationary.

S. O. Krichak (✉) · P. Alpert · P. Kunin
Department of Geophysics and Planetary Sciences,
Raymond and Beverly Sackler Faculty of Exact Sciences,
Tel Aviv University, Tel Aviv, Israel
e-mail: shimon@cyclone.tau.ac.il

**Keywords** Regional climate modeling · Eastern Mediterranean · Model configuration · Coastal zone · Offshore precipitation

## 1 Introduction

Climate of the eastern Mediterranean (EM) region and especially that of the Eastern Coastal Mediterranean (ECM) zone is characterized by changeable rainy weather with moderate temperatures during the cool seasons, and dry and hot weather during summer. The conditions fit the "Mediterranean" type of the Köppen and Geiger's (1936) classification. They are significantly determined by the region's location in the zone dominated by polar front activity in winter, and by a subtropical high-pressure system during summer. The EM region's climate is strongly influenced by the effects of annual variations of the Asian monsoon (Bedi et al. 1976; Hasanean 2005; Rodwell and Hoskins 1996; Ziv et al. 2004). During the cool season, the EM climate is affected by specific synoptic processes associated with interaction of the upper-troposphere jet stream with the regional terrain over northern Africa (Krichak et al. 1997). Especially important for the EM climate is the contribution of heavy precipitation events (HPE). Over coastal zone of the EM the HPE are usually associated with landfall of baroclinic systems that direct strong and moist low-level flow against the terrain from the sea. When the cyclones approach the coast, cloud development and precipitation are influenced by local topography.

The EM region is part of a continental system extending from south-western to south-eastern Europe (in its northern part) to central Asia and north-eastern Africa (in its eastern and southern parts). It is characterized by substantial

differences in the amounts of solar radiation between its northern and southern parts. Effects of local topography/sea/vegetation mainly lead to sharpening gradients in the distributions of main climate parameters (especially in the immediate coastal area). A large part of the EM air moisture originates from the North Atlantic and Arabian Sea areas (Lionello et al. 2006). The Mediterranean Sea itself (due to its zonal orientation between three continents) and other water basins of the area also serve as important sources of heat, water vapor and latent heat for synoptic processes here (Lionello et al. 2006; Trigo et al. 1999).

Winters in the EM are characterized by passing disturbances known as Cyprus cyclones and, during periods without them, intrusions of high pressure systems and polar air masses (Alpert et al. 1990; Saaroni et al. 1996; Levin and Saaroni 1999). During summer, the EM is under the influence of a quasi-stationary Persian Gulf trough system that extends from the area of the Indian monsoon low, and, in the southern parts, is strongly affected by a ridge from the Azores anticyclone. The EM weather under the Persian trough conditions is characterized by westerly winds and formation of a diurnal breeze mechanism in the lower (about 1,000 m) layer. Above the lower layer, the atmospheric conditions are dominated by the effects of subtropical anticyclones causing subsidence and an almost absolute absence of rainfall (Bitan and Saaroni 1992) from mid-June to mid-September.

Several major synoptic processes determine the region's climate during intermediate seasons. Among those the most important are Sharav cyclones and Red Sea Trough systems. The Sharav cyclones (thermal low pressure North African systems) move rapidly along the North African shore area, especially during spring. They cause very high temperatures and low humidity when the EM is ahead of and below the warm sector of cyclone (Alpert et al. 1999; Saaroni et al. 1998). The Red Sea Trough (RST) is common in both spring (less typical) and autumn (Ashbel 1938; El-Fandy 1948; Krichak et al. 1997; Tsvieli and Zangvil 2005; Ziv et al. 2005). The RST is an extension of the African monsoon trough. Intensity of the weather processes associated with the RST is significantly determined by the position of the Inter-Tropical Convective Zone (ICTZ). During October and April, the ITCZ is located approximately at 15°N–20°N (along meridian 0°E). The RST is a low-level trough extending from the Red Sea northward. The air-flow in the EM depends on the location of the trough's axis (Dayan 1986). The EM weather conditions associated with the RST systems are usually dry. HPE's are typical however in the cases of development of so called Active Red Sea Troughs (Kahana et al. 2002), with a lower-level RST accompanied by distinct upper-level trough extending from the eastern Mediterranean towards the Nile River, roughly along the 30°E meridian. In such synoptic situations, the southern part of the EM is positioned under the inflection point ahead of the trough, where favorable conditions for rain formation, i.e. positive vorticity advection, take place.

Existence of the EM offshore precipitation zone as a typical peculiarity of the EM climate has been noted. Based on radar measurements, Levin et al. (2004) conclude that in the Tel Aviv area in winter up to three times more rain is falling over sea than over land. Gridded data sets available (Beck et al. 2005; Mitchell et al. 2004; New et al. 2000; Yatagai et al. 2008), that are based on terrestrial observations, are insufficient to confirm the observation. The peculiarity of the EM climate has been attributed to air-see temperature gradients (Khain et al. 1996). During the cool season when the EM precipitation takes place the sea surface temperature (SST) is higher than the land surface temperature by 5–10°C. The temperature difference is sufficient to form land breeze–like circulation which interacts with dominating westerlies and leads to intensified cloud formation over the sea $\sim$10–20 km westward of the coastal line (Khain et al. 1993; Khain and Sednev 1996; Khain et al. 1996).

Another physical mechanism may also be acting. Formation of offshore precipitation zones has been noted in the near coastal zones experiencing weather conditions associated with eastward moving cyclones. Formation of offshore precipitation zones have been documented in the synoptic processes over the Alpine and South California regions (Buzzi et al. 1998; Houze et al. 2001; James and Houze 2005). The effect has been attributed to the weather processes taking place in the areas, where terrain contains meridionally oriented mountain ridges (approximately orthogonal to the prevailing low-level flow). In the cases, when fronts approach the coast, moist air belts are often oriented almost perpendicular to the two-dimensional ridges of the coastal mountains. Such orientation of the mountain ridges characterizes also the northern and central parts of the EM region. To the best of the authors' knowledge no analysis of the topographical offshore precipitation in the EM has been yet performed. One of the main goals of the study was to evaluate a possible role of topography effects in precipitation distribution and formation of offshore precipitation zone over the near coastal EM.

The roles of different mechanisms determining distribution of precipitation over the EM region are investigated here based on results of a series of regional climate simulation experiments. The use of regional climate modeling (RCM) approach to downscale results of coarse-resolution global climate simulations has become an accepted strategy (e.g. Christensen and Christensen 2003; Giorgi and Mearns 1999; Takle et al. 2007; Pal et al. 2007). Different RCMs are not equally successful in reproducing climate of some regions, however (Takle et al. 2007). The level of accuracy

of climate representation by different models depends on the choice of physical parameterizations (Jacob and Podzun 1997), domain size (Seth and Giorgi 1998; Vannitsem and Chome 2005), lateral boundary-nesting effects (Caya and Biner 2004), effects of terrain, contribution of smaller-scale processes in the regional climates (Krichak et al. 2007), etc. Relative importance of the factors may differ depending not only on geography of a region with its topography, land-sea-atmosphere interaction effects, and other physically-acting mechanisms, but also on typical (both inside and outside of the domain) synoptic processes contributing to its climate. Only a limited number of efforts to simulate the EM climate have been made up to now (Alpert et al. 2008; Evans et al. 2004; Gao et al. 2006; Giorgi et al. 2004; Krichak et al. 2007).

The motivation for this study was two-fold: a) to estimate the relative roles of large scale effects, breeze circulation in the near coastal zone and topography effects in the development of offshore precipitation zone in the EM coastal zone; to evaluate sensitivity of results of representation of seasonal distribution of precipitation over the EM region using an RCM model. Description of the model and details of the experiments' setup are provided in Sect. 2. Results of the climate simulation experiment are presented in Sects. 3 and 4. Discussion and conclusions are given in Sect. 5.

## 2 Modeling details and design of experiments

The model adopted is a third generation RegCM3 model (Pal et al. 2007) with 14 vertical $\sigma$-levels (five levels located below $\sim$1,500 m), 50 km horizontal spacing and model top at 80 hPa. The lateral boundary relaxation zone covers 11 grid intervals. A smoothing of terrain inside of the relaxation zone is performed. The physical options chosen [radiation (Kiehl et al. 1996); land-surface model (Dickinson et al. 1993; Gao et al. 2006); planetary boundary layer (Holtslag et al. 1990); ocean flux parameterization (Zeng et al. 1998), lateral boundary treatment (Davies and Turner 1977); cumulus parameterization according to Grell (1993) with Fritsch and Chappell (1980) closure—for references see Pal et al. (2007)] are selected based on results of earlier analyses (Giorgi et al. 2004; Krichak et al. 2007). The standard strategy (Christensen et al. 1997; Vannitsem and Chome 2005) of using perfect boundary conditions was adopted to reduce the errors coming from the Lateral Boundary Conditions (LBC). The LBCs are fed to the model every 6 h from NCEP-NCAR reanalysis data (NNRP) (Kalnay et al. 1996) available with 2.5° horizontal spacing.

Ten RCM experiments differing by the length of the period of simulation and the choice of the cumulus parameterization schemes adopted have been performed. In Exp 1–Exp 6 the downscaling RegCM3 runs are performed from 00:00 UTC 1 January 1986 to 31 December 1987 using six version of domain configuration (A–F), respectively. The two-year time period has been characterized by exceptionally intense November-December precipitation over the ECM (Krichak et al. 2000). The aim of the simulation experiments was to isolate the effects of model domain and location of lateral boundary choices in results of the RCM simulations of precipitation distribution over the EM region.

In the following analysis the monthly-mean precipitation amounts (as well as the seasonal and annual ones) simulated over the area 25°N–40°N, 25°E–40°E (approximately representing the EM region) are compared with those from the gridded datasets of Climate Research Unit (CRU) of the University of East Anglia, UK (Mitchell et al. 2004; New et al. 2000) and Variability Analyses of Surface Climate Observations (VASClimO) at the Global Precipitation Climatology Centre (GPCC) (Beck et al. 2005). Both the CRU and VASClimO data are available with 0.5° resolution over the land areas only.

The too short (2-year) period of the Exp 1–Exp 6 simulations could be affecting the results. Four (Exp 7–Exp 10) additional model simulations been performed for a 13-year period (January 1 1982–31 December 1994) to confirm the conclusions obtained and evaluate the role of physical parameterizations chosen. It may be noted here that the January 1 1982–31 December 1994 period has been characterized by two (El Chichon, April 4, 1982 and Pinatubo, June 15, 1991) low-latitude volcanic eruptions, which have influenced European-Mediterranean region via a notable Arctic Oscillation response (Stenchikov et al. 2006). No evaluation of the role of volcanic eruptions in the EM climate oscillation has been performed here however. Three different model domains (A, C, D) are used in Exp 7–9, respectively. Exp 10 consists of realization of additional 13-year RCM simulation of the ECM climate. A model configuration (denoted as RegCM3-M in the following) using cumulus parameterization according to Grell (1993) with Arakawa and Schubert (1974) closure and a model domain D was adopted in the experiment.

The referenced above model domains (A–F) are shown in Fig. 1. Here, domain A (Exp 1 and Exp 7) with 48 $\times$ 58 grid-points covers a relatively small part of the eastern Mediterranean (EM, North Africa in the south to the Black Sea in the north; Southern Italy in the west, and close to the Caspian Sea- Persian Gulf area in the east). Domain B (Exp 2) has 100 $\times$ 100 grid points and covers a large area that includes most of Western Europe, the Mediterranean Sea, the Caspian Sea, and part of the Persian Gulf. The other three domains C (Exp 3 and Exp 8); D (Exp 4, Exp 9 and Exp 10); E (Exp 5) have 80 $\times$ 80 grid points and are configured by shifting the centers of the domains eastward

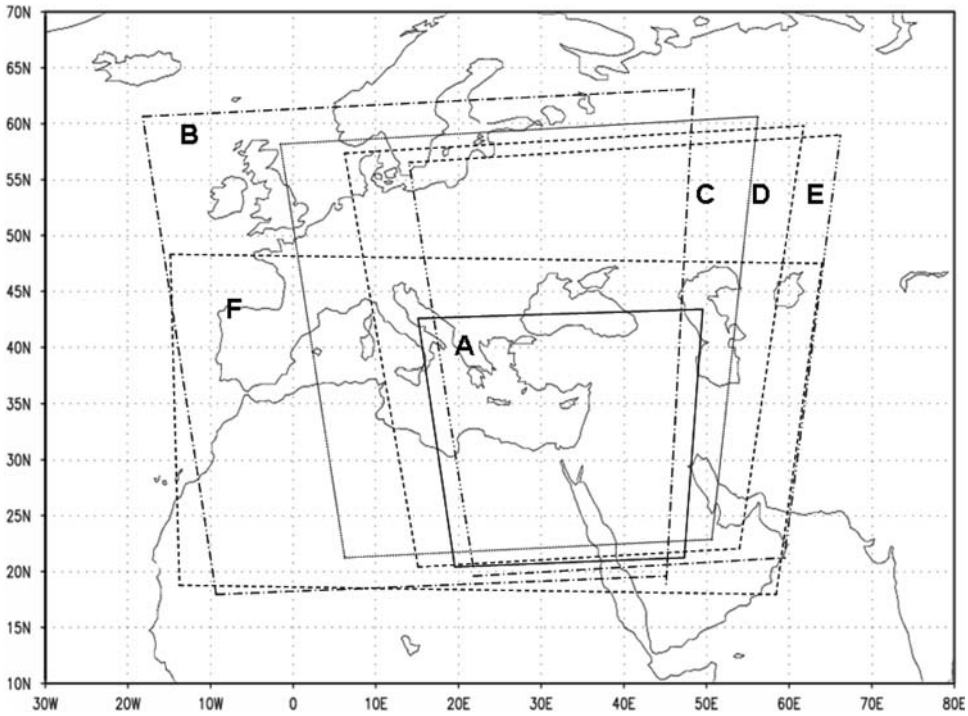


**Fig. 1** Six (A–F) domain configurations used

by ~7°. The last of the domains tested F (Exp 6) has 70 × 130 grid points, and covers an area that includes the Pyrenean Peninsula, the Mediterranean Sea, as well as Black and Caspian Seas. The eastern boundary of domain F coincides with that of domain E.

## 3 RCM results

### 3.1 Two-year sensitivity evaluations

#### *3.1.1 Spatial distribution of precipitation*

Patterns with the differences between the simulated annual (from December 1986 to November 1987) and corresponding CRU precipitations (interpolated to the model grid) are given in Fig. 2a–f, respectively. A positive (negative) bias in the model representation of precipitation over the northern (central and southern) part of the area may be indicated. Significant differences over offshore area characterize the results. To allow evaluation of the RCM results over the sea, patterns with those from the individual experiments (Exp 1–6) are also presented (Fig. 3a–f). A maximum of ~700 mm in the annual ECM precipitation is reached in Exp 1 (Fig. 3a). Simulated precipitation is significantly more intense (maximum of ~1,200–1,300 mm) in Exp 2 (Fig. 3b). The maximum precipitation produced in Exp 3 (Fig. 3c) is of the same order as that in Exp 1, but the zone with the rains is shifted eastward. Maxima in the annual precipitation in Experiments 3–5 (Fig. 3d–f) are also of about 800–900 mm.

Observed during the period annual precipitation (according to the CRU and VASClimO datasets) is presented in Fig. 4a,b. A good level of agreement between the two sources may be noted. To allow evaluation of the accuracy of representation of precipitation by the gridded datasets, a spatial pattern of mean Jackknife-error (e.g. Heltshe and Forrester 1985) for October 1986–April 1987 based on the VASClimO data, is also provided (Fig. 4c). Most of the ECM area is satisfactorily (except for the north-eastern part of the coastal zone) covered by the observation data. Similar level of reliability (not presented) characterizes also the CRU-based data.

Precipitation patterns from Exp 1–Exp 6 (Fig. 3a–f) significantly differ over the north-eastern part of the EM area. About 1,000–1,100 mm of precipitation (Fig. 3a) is simulated here in Exp 1 (~600 mm according to the CRU data). Less intense precipitation is simulated in Exp 2–Exp 6. Results of Exp 4 and 5 (Fig. 3c,d) appear to reproduce the actual precipitation pattern with the most accuracy (Fig. 7a,b). A notable underproduction of precipitation over the land area is evident in results of Exp 1–Exp 3 (Fig. 3a–c). More successful are the results of Exp 4–6 (Fig. 3d–f).

Existence of offshore precipitation zone characterizes results of all the experiments. The zone appears to be a typical peculiarity of the simulated in the experiments ECM climate.

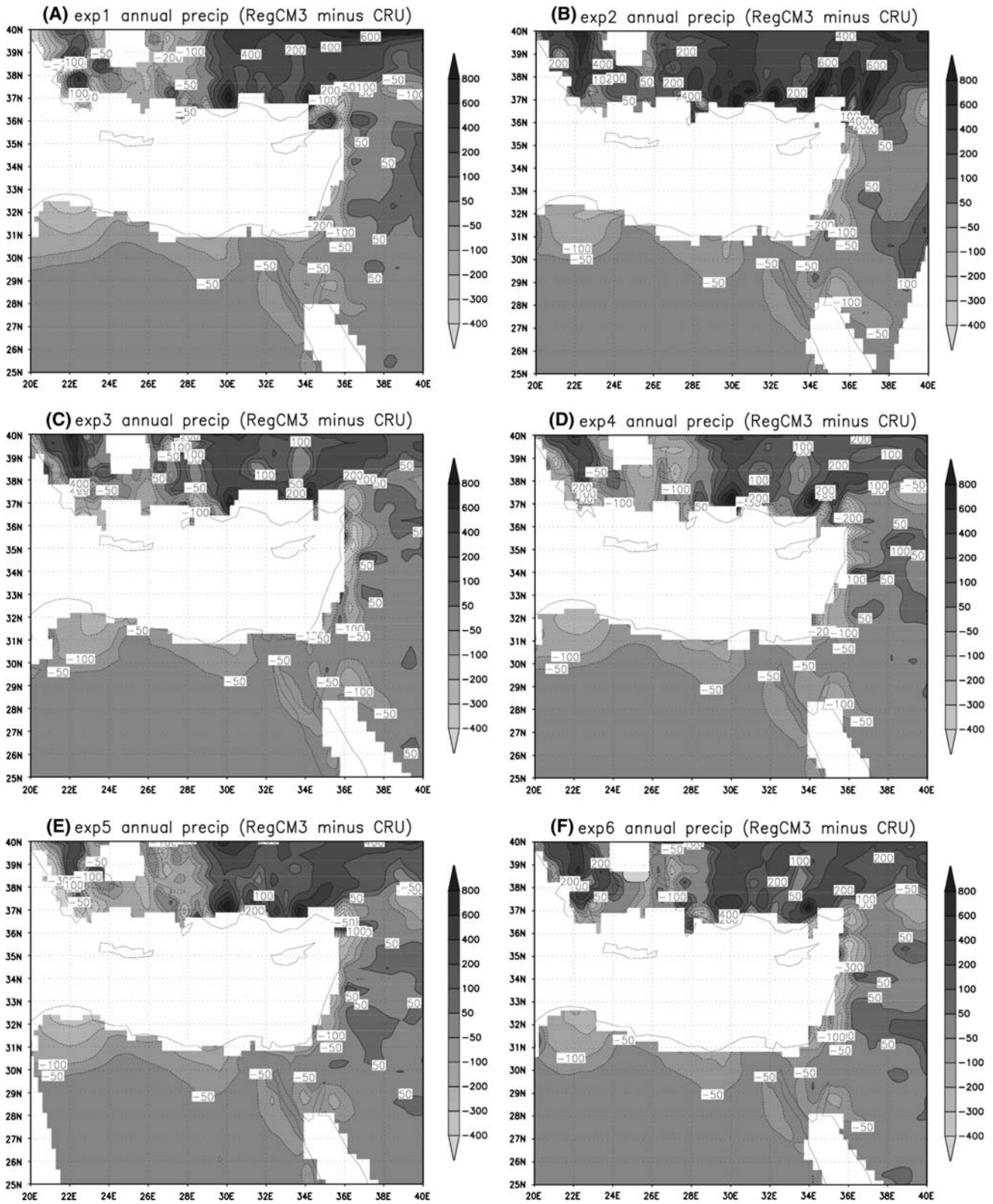


**Fig. 2** Difference between the simulated and actual (CRU) annual precipitation (mm) (**a**–**f**) for Exp 1–Exp 6, respectively

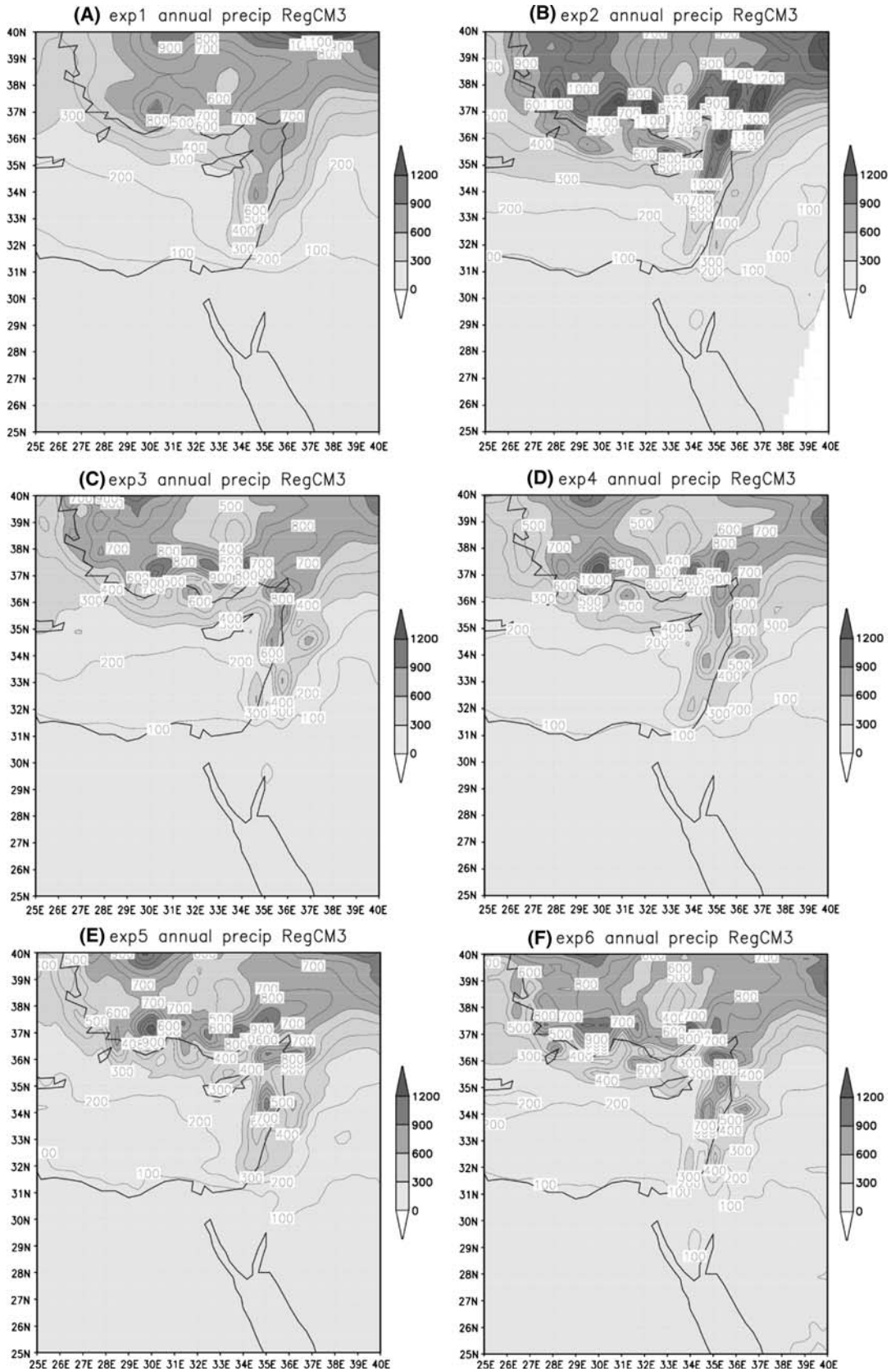


**Fig. 3** Annual precipitation (cm) during December 1986–November 1987 simulated with the RegCM3 model over the EM region (**a**–**f**) predicted in Exp 1–Exp 6, respectively

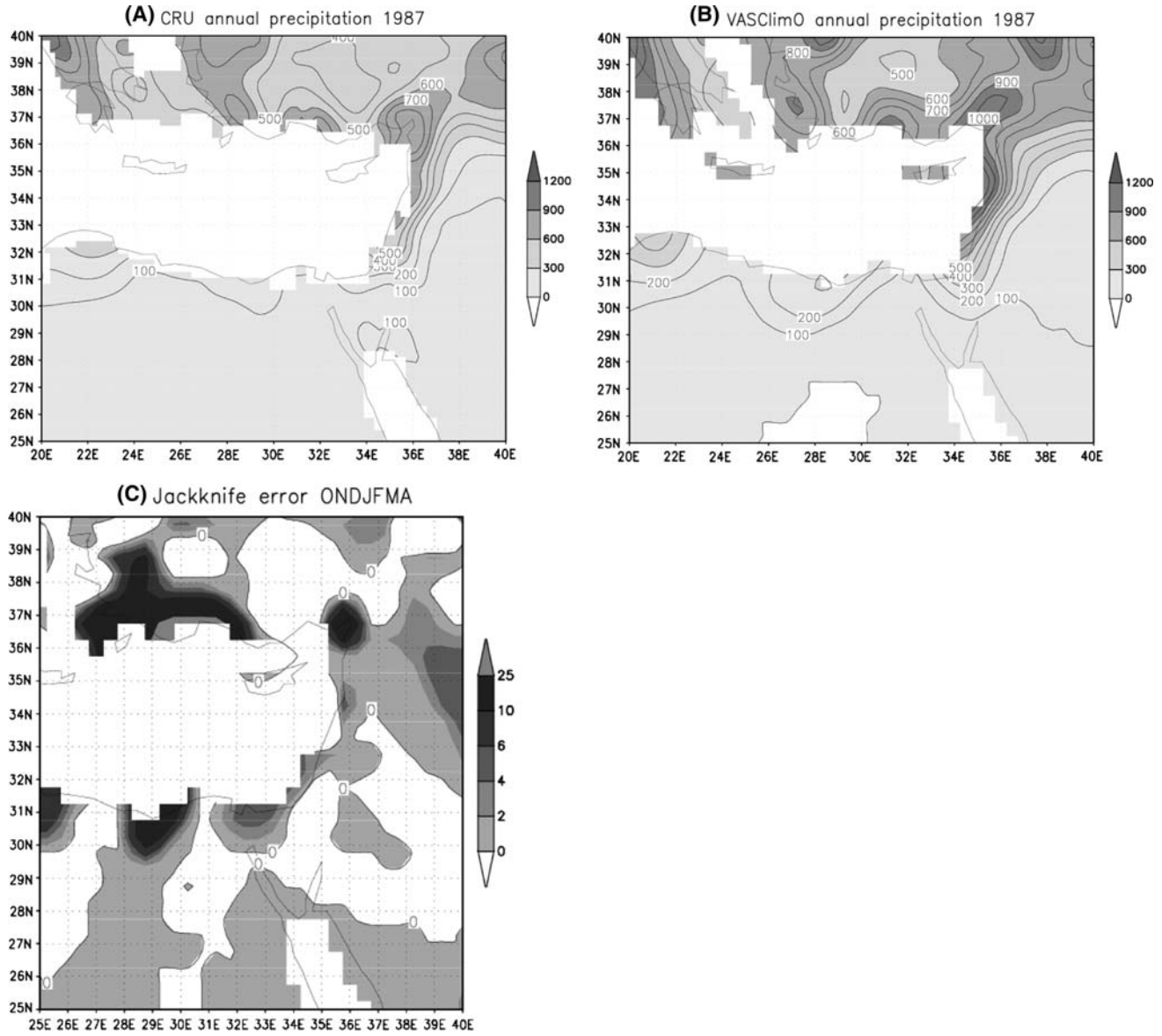


**Fig. 4** Annual precipitation (cm) according to **a** CRU, **b** VASClimO data, **c** spatial distribution of mean Jackknife-error (VASClimO), during December 1986–November 1987

### *3.1.2 Annual variation of precipitation and temperature*

Correlations between the simulated (Exp 1–Exp 5) area-mean daily precipitation (*Prec*) and air temperature at 2 m (*T2 m*) and corresponding area-averaged observation data (Tables 1 and 2), respectively (both statistically significant at 0.05% confidence level according to the *t*-test) provide additional information. Results of Exp 10 have not been included in this evaluation due to the practically identical position of the eastern boundary in domains E and F. The simulated daily-mean values of the *T2 m* and *Prec* in Israel (averaged over 32°30′–34°N; 34°30′–36°E) are verified here against observation data at several stations over central Israel (for precipitation—six meteorological stations with coordinates: 33°14′N,35°34′E; 33°10′N,35°36′E; 33°04′N,35°27′E; 33°03′N,35°13′E; 32°43′N,35°34′E; 32°59′N,35°30′E; for 2-m air temperatures—at two stations with coordinates: 32°58′N,35°30′E; 32°01′N,34°25′E.)

The highest values (0.65 and 0.67) of the correlations between the model-simulated and observed *Prec* values correspond to Exp 1 (domain A) and Exp 4 (domain D), respectively (Table 1). The advantage of domain D is even more apparent when the correlations are calculated for the situations with precipitation intensities greater than 0.5 mm day$^{-1}$ and 1.0 mm day$^{-1}$, respectively (0.56 and 0.55).

**Table 1** Correlations between observed daily average precipitations at five stations in northern Israel and simulations for the same area

| Exp | A | B | C | D | E |
|---|---|---|---|---|---|
| All | 0.65 | 0.52 | 0.61 | 0.67 | 0.62 |
| Prec $\geq$ 0.5 mm | 0.51 | 0.35 | 0.49 | 0.56 | 0.54 |
| Prec $\geq$ 1.0 mm | 0.49 | 0.39 | 0.47 | 0.55 | 0.52 |

**Table 2** Correlations between observed daily 2-m air temperatures at two stations in Israel and simulations for the same area

| Exp | A | B | C | D | E |
|---|---|---|---|---|---|
| 2 m air temp | 0.93 | 0.90 | 0.94 | 0.94 | 0.92 |

Simulated air temperatures are significantly less sensitive however to the variations in the model domain parameters. Only minor differences characterize the accuracy of the model representation of the *T2 m* values (Table 2). The highest values of the correlation (0.94) characterize results of Exp 3 (domain C) and Exp 4 (domain D).

### *3.1.3 Role of neighboring sub-areas*

To evaluate the role of precipitation simulated over different parts of the region to that of the ECM, the area of analysis is divided to seven sub-areas schematically indicated in Fig. 5. Topography of the EM region is also given in the figure. The ECM is represented here by the sub-area 6. Sub-areas 3 and 4 represent the northern and northeastern parts of the northern EM region, respectively. Correspondingly, sub-areas 1 and 5 in Fig. 5 represent the area of Caucasus, and sub-area 7—the Middle East. It may be noted that sub-areas 1, 3, 4, and 5 are characterized by steep topography. Also quite steep topography (not indicated in Fig. 5) characterizes some parts of the EM coastal zone.

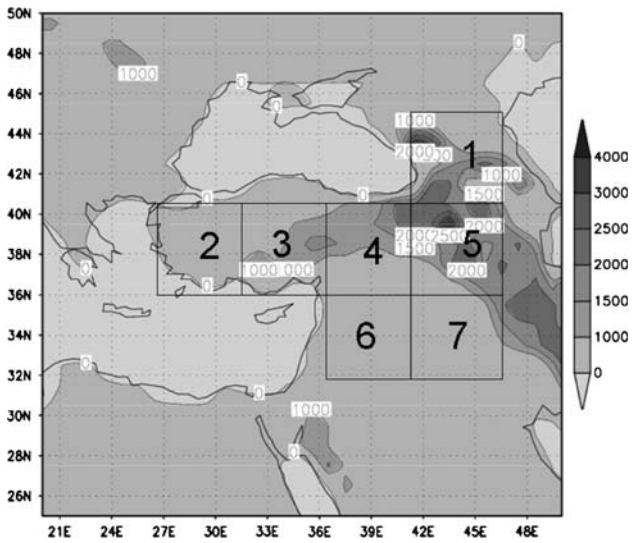


**Fig. 5** Topography of the region (m) together with seven sub-areas for evaluation of the simulation accuracy

Monthly mean values of Root-Mean Square Differences (RMSD) between the simulated precipitation and interpolated to the model grid-points CRU data have been calculated for each of sub-areas 1–7. Mean correlations $R$ between the RMSD values for the 1, 2, 3, 4, 5 and 7 sub-areas and those in sub-area 6 (ECM) (statistically significant at 1% level) are presented in Table 3. Here, the RMSD values from Exp 4–6 (domains D, E, F) over sub-area 6 are well correlated with those over sub-areas 7 ($R = 0.9$) and 4 ($R = 0.8$) (Exp 3 and 4, domains C, D). The evaluation concludes that domain D is among those producing the best results. The mean (for all experiments) values of the correlations (Table 3) show that accuracy of representation of real precipitation over sub-areas 4 and 7 plays the most important role in ensuring the accuracy of representation of the ECM precipitation.

## 3.2 Thirteen-year RCM sensitivity evaluations

Additional four RCM downscaling experiments have been performed to deeper investigate synoptic mechanisms responsible for formation of the offshore precipitation zone. Produced in Exp 7–Exp 9 multi-year annual precipitation patterns using domains A, C, D are given in Fig. 6a–c, respectively. Simulated annual precipitation pattern from Exp 10 (D domain) is also presented (Fig. 6d) to allow evaluating the effects of convective parameterization.

The offshore precipitation is simulated in all the experiments. As above, the model results are sensitive to domain choice. Precipitation in the zone is relatively weak (400 mm) in results of Exp 7 using domain A (Fig. 6a). Almost unrecognizable the offshore zone of precipitation is in Fig. 6b (Exp 8, domain C). Practically identical the multi-year mean annual precipitation patterns are in Fig. 6c

**Table 3** Correlations (statistically significant at 1% level) of root mean square differences between simulated and real (CRU) annual precipitation over sub-areas 1–5 and 7 with those over sub-area 6

| Sub-area/experiment | 1 | 2 | 3 | 4 | 5 | 7 |
|---|---|---|---|---|---|---|
| 1 (domain A) | 0 | −0.1 | 0.2 | 0.6 | 0.4 | 0.7 |
| 2 (domain B) | −0.2 | 0.1 | 0.3 | 0.6 | −0.1 | 0.5 |
| 3 (domain C) | −0.4 | 0 | 0.3 | 0.8 | 0.7 | 0.8 |
| 4 (domain D) | −0.2 | 0.3 | 0.5 | 0.8 | 0 | 0.9 |
| 5 (domain E) | −0.3 | 0.2 | 0.6 | 0.7 | 0.3 | 0.9 |
| 6 (domain F) | −0.2 | 0.1 | 0.3 | 0.7 | 0.3 | 0.9 |
| Mean | −0.22 | 0.1 | 0.37 | 0.7 | 0.27 | 0.78 |

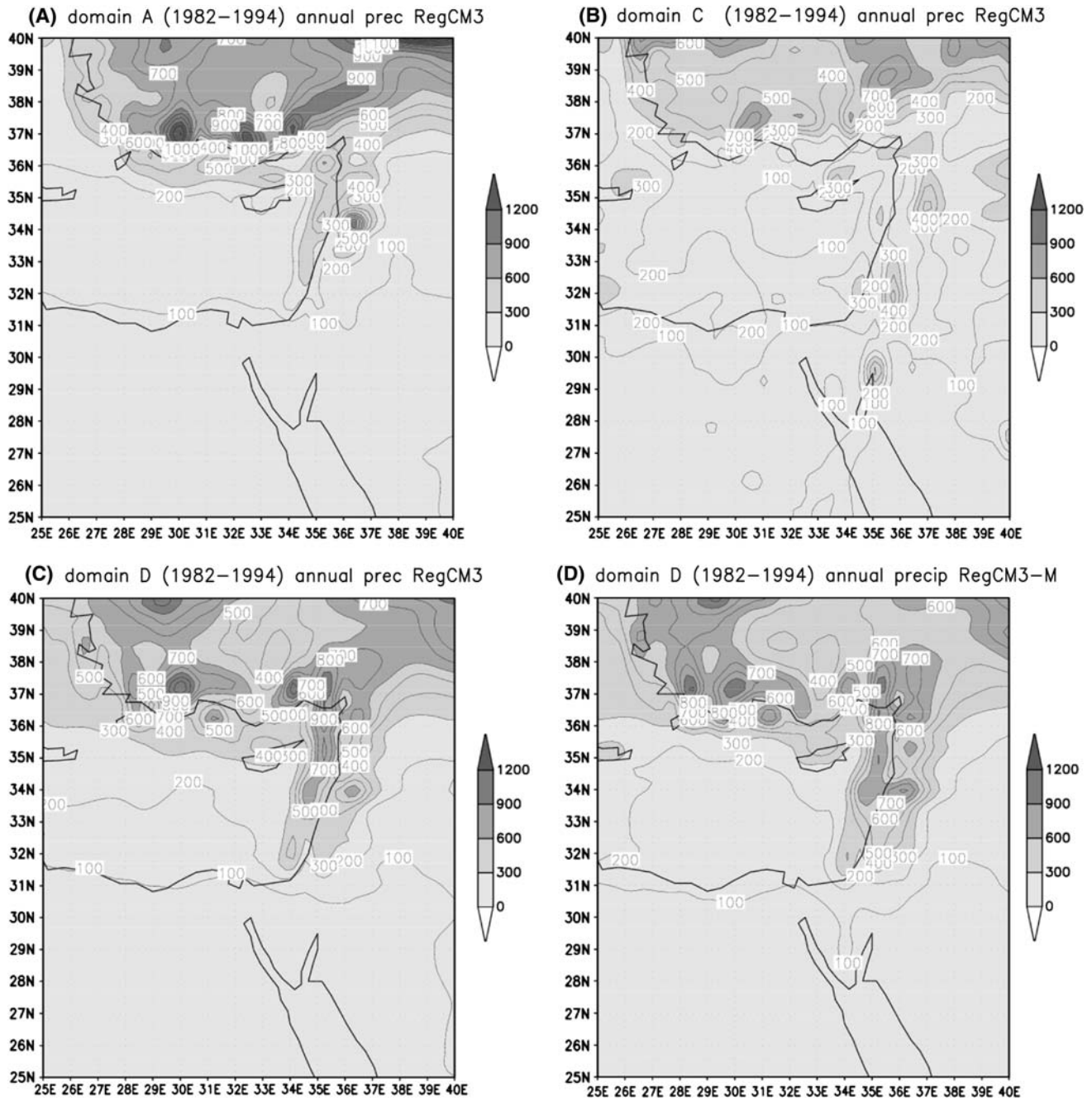


**Fig. 6** Multi-year (1982–1994) annual precipitation (mm) using RegCM3 with **a** domain (A, Exp 7), **b** domain (C, Exp 8), **c** domain (D, Exp 9), **d** domain (D, Exp 10)

(Exp 4) and 6d (Exp 9), both using domain D, but differing by the choice of the cumulus parameterization scheme. Intensity of the simulated offshore precipitation appears to be not sensitive to choice of the physical parameterization approach.

There are no significant differences between the results of simulations for 2-year and 13-year periods. Comparison of the corresponding figures (Figs. 3a and 6a; Figs. 3c and 6b; Figs. 3d, and 6c) leads to the conclusion that the main effects of the model domain choice are already apparent in the results of the 2-year experiments. Dependency of location and intensity of the simulated ECM offshore precipitation zone on the choice of the domain version is evident. The differences due to the employment of different cumulus parameterization schemes (Fig. 6c,d) are much less significant over the EM than those due to the use of the different domains. The use of the modified (RegCM3-M) model version allows, however, reduction of

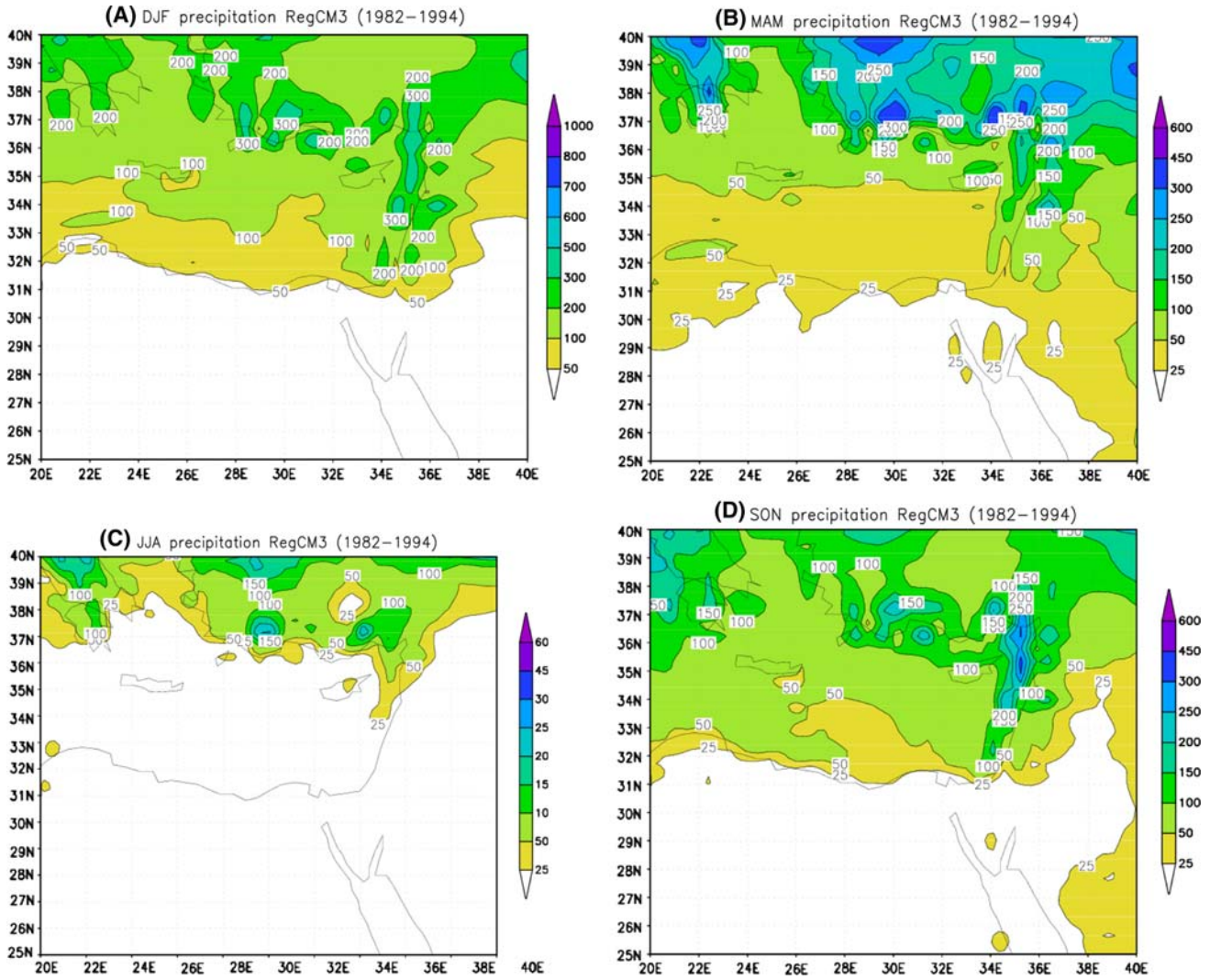


**Fig. 7** Mean multi-year (1982–1994) seasonal precipitation (mm) simulated in Exp 10 for **a** DJF, **b** MAM, **c** JJA, **d** SON

an earlier detected (Krichak 2008; Krichak et al. 2009) positive bias in the simulated warm-season precipitation over South Eastern Europe (not presented).

## 4 Interannual variation of the simulated precipitation

Due to similarity of results of Exp 7–Exp 10, interannual variations of the simulated seasonal precipitation over the EM region are analyzed here based on results of only one (Exp 10) of the ten experiments performed. Figure 7a–d present multi-year mean seasonal precipitation patterns for winter (December-March, DJF), spring (March-May, MAM), summer (June-August, JJA), and autumn (September–November, SON), produced in the experiment. Simulated and actual DJF precipitation patterns are given in Fig. 7a. As was already indicated, in addition to the precipitation zone along the coastal part of the ECM the model-produced pattern also contains the offshore precipitation zone located about 60–100 km westward of the eastern coast of the Sea.

The simulated MAM precipitation is given in Fig. 7b. As earlier, the pattern is characterized by an offshore precipitation zone along another one over land. Amount of precipitation over the ECM offshore zone is significantly higher than that over the land area. A minor offshore precipitation zone is also simulated for JJA (Fig. 7c). The SON pattern (Fig. 7d) is characterized by a zone with intense precipitation about 60 km westward of the coastal line.

An annual variation in precipitation amount in the offshore zone is evident. During DJF (Fig. 7a), simulated offshore precipitation is weaker (250–300 mm), than during SON. The spring-time offshore precipitation (Fig. 7b) is clearly less intense (50–150 mm) than those for DJF and SON (Fig. 7a,d). The simulated offshore precipitation is

characterized by a notable intra-annual variability. The highest intensity of the offshore rains (250–400 mm) is simulated for the SON season (Fig. 7d). Here, the zone extends along the whole ECM area from its northern to the southern parts. Almost no SON precipitation is simulated over the land. Over the land, simulated MAM precipitation is stronger than the offshore one.

## 5 Discussion

Results of all the experiments are characterized by an underproduction of precipitation over the central and southern parts of the EM, especially notable during the autumn and winter (not presented) seasons. A notable overproduction of precipitation characterizes the model results over the northern part of the EM however. The offshore precipitation zone is found in results of all the experiments performed. Performed evaluations demonstrate dependence of the RCM results on the choice of the model domain. Intensity of precipitation as well as positioning of the simulated zone are also sensitive to the choice of the model domain, Simulated offshore precipitation zone is underdeveloped in results of the RCM experiments 3 and 8 (domain C). On the contrary, results of Exp 4 (domain A) and Exp 5 (domain B) are characterized by unrealistically intense offshore precipitation zone.

When using a relatively small model domain (A), the simulated ECM precipitation zone is located several dozens of kilometers westward of its actual position. The ECM precipitation is notably more intense in experiments with a large model domain (B), having its eastern boundary approximately along the same meridian ($\sim$45°E) as that in domain A. The precipitation zone is shifted further eastward in the results of Exp 4, using a large enough domain (C), with its eastern boundary placed along $\sim$50°E. Results of the most successful model representation of the actual EM precipitation pattern are obtained in Exp 4 using domain D (with eastern boundary along $\sim$52°E). The ECM precipitation zone is simulated with also reasonable accuracy in Exp 5 and Exp 6, using model domains (E, F) (both having their eastern lateral boundaries along $\sim$59°E). In may be concluded that the modeling results are practically insensitive to the positioning of the western boundary of the model domain. However, positioning of the northern and especially eastern boundaries significantly affects that of the ECM precipitation zone in the six downscaling experiments for 1986–1987.

According to the results, the accuracy of representation of the seasonal as well as annual precipitation in ECM is quite sensitive to that over the mountainous area in northern part of the Asia Minor. It is interesting to note the negative (although low) correlation between RMSD over sub-area 1 (Caucasus) with that over the EM. Overproduction of precipitation over the Caucasus appears to be the cause of the earlier indicated negative bias in the model representation of the actual precipitation in the EM. Representation of the ECM precipitation (and of the offshore precipitation zone in particular) by the model is strongly affected by that of the accuracy of reproducing of actual precipitation distribution over the area to the south of the Black-Caspian Seas and Himalayan-Alpine Mountain ridge.

The level of success of the model representation of the actual precipitation over the ECM appears to be depending on that of precipitation balance over different parts of the domain. Excessive moisture convergence over a sub-area usually takes place at the expense of moisture divergence from neighboring areas.

The following explanation of the results may be suggested. As was already notified, rainy events over the EM usually take place during synoptic periods characterized by intense north-westerly air flows of European or east Siberian origin to the EM (Ziv et al. 2006). While moving over warmer Mediterranean, the air masses gain moisture and become conditionally unstable. With upper troughs remaining quasi-stationary, the periods of the cold air transport may be quite long. In the near coastal offshore EM zone, where SSTs (and near surface air temperatures) are higher and the breeze-like Khain et al. (1993) mechanism (due to the land-sea air temperature differences) is acting, developments of secondary cold frontal zones and persistent squall lines take place. Effects of orography are responsible for formation of the second precipitation zone over the coast (Gao et al. 2006). The differences in experiments' results are resulting from those in intensity of the air mass transport.

**Acknowledgments** The helpful comments by two anonymous reviewers are acknowledged with gratitude. The research was supported by the German-Israeli research grant (GLOWA-Jordan River) from the Israeli Ministry of Science and Technology, the German Bundesministerium fuer Bildung und Forschung (BMBF), the Water Authority of Israel (Project No. 0603414981), and by integrated project granted by the European Commission's Sixth Framework Programme, Priority 1.1.6.3 Global Change and Ecosystems (CIRCE), Contract no.:036961. The authors are grateful to the Physics of Weather and Climate (PWC) Section of the Abdus Salam International Centre for Theoretical Physics (ICTP), Trieste, for providing expertise on using RegCM3. We would also like to thank Dr. Peter Mayes, New Jersey Department of Environmental Protection, USA, for his contribution in editing the manuscript, as well as Anat Baharad and Netta Tzur for their help in processing of the simulation results. The authors also acknowledge fruitful discussions and helpful comments by Dr. Yoseph Barkan.

## References

Alpert P, Ziv B (1989) The Sharav cyclone—observations and some theoretical considerations. J Geophys Res 94:18495–18514

Alpert P, Neeman BU, Shay-El Y (1990) Climatological analysis of Mediterranean cyclones using ECMWF data. Tellus 42A:65–77

Alpert P, Krichak SO, Shafir H, Haim D, Osetinsky I (2008) Climatic trends to extremes employing regional modeling and statistical interpretation over the E Mediterranean. Glob Planet Change 63:163–170

Arakawa A, Schubert WH (1974) Interaction of a cumulus cloud ensemble with the large-scale environment; Part I. J Atmos Sci 31:674–701

Ashbel D (1938) Great floods in Sinai Peninsula, Palestine, Syria and the Syrian desert, and the influence of the Red Sea on their formation. Q J Roy Meteorol Soc 64:635–639

Beck C, Grieser J, Rudolf B (2005) A new monthly precipitation climatology for the global land areas for the period 1951 to 2000. Climate Status Report 2004, pp 181–190. German Weather Service, Offenbach

Bedi HS, Datta RK, Krichak SO (1976) Numerical forecast of summer monsoon flow patterns. Soviet meteorology and hydrology 5, New York, pp 39–45

Bitan A, Saaroni H (1992) The horizontal and vertical extension of the Persian Gulf pressure trough. Int J Climatol 12:733–747

Buzzi A, Tartaglione N, Malguzzi P (1998) Numerical simulation of the 1994 Piedmont flood: role of orography and moist processes. Mon Weather Rev 126:2369–2383

Caya D, Biner S (2004) Internal variability of RCM simulations over an annual cycle. Clim Dyn 22:33–46

Christensen JH, Christensen OB (2003) Climate modeling: severe summertime flooding in Europe. Nature 421:805–806

Christensen JH, Machenhauer B, Jones RG et al (1997) Validation of present-day regional climate simulations over Europe. Clim Dyn 13:489–506

Davies HC, Turner RE (1977) Updating prediction models by dynamical relaxation: an examination of the technique. Q J Roy Meteorol Soc 103:225–245

Dayan U (1986) Climatology of back-trajectories from Israel based on synoptic analysis. J Clim Appl Meteorol 25:591–595

Dickinson RE, Henderson-Sellers A, Kennedy PJ (1993) Biosphere-Atmosphere Transfer Scheme (BATS) version 1E as coupled to the NCAR community climate model, Tech. Rep. TN-387 + STR, NCAR, Boulder, 72 p

El-Fandy MG (1948) The effect of the Sudan monsoon low on the development of thundery conditions in Egypt, Palestine and Syria. Q J Roy Meteorol Soc 74:31–38

Evans JP, Smith RB, Oglesby RJ (2004) Middle East climate simulation and dominant precipitation processes. Int J Climatol 24:1671–1694

Fritsch JM, Chappell CF (1980) Numerical prediction of convectively driven mesoscale pressure systems. Part I: convective parameterization. J Atmos Sci 37:1722–1733

Gao X, Pal JS, Giorgi F (2006) Projected changes in mean and extreme precipitation over the Mediterranean region from a high resolution double nested RCM simulation. Geophys Res Lett 33: L03706. doi:10.1029/2005GL024954

Giorgi F, Mearns LO (1999) Introduction to special section: regional climate modeling revisited. J Geophys Rev 104(D6): 6335–6352

Giorgi F, Bi X, Pal JS (2004) Mean, interannual variability and trends in a regional climate change experiment over Europe. I. Present-day climate (1961–1990). Clim Dyn 22:733–756

Grell GA (1993) Prognostic evaluation of assumptions used by cumulus parameterizations. Mon Weather Rev 121:764–787

Hasanean HM (2005) Variability of teleconnections between the Atlantic subtropical high and the Indian monsoon low and related impacts on summer temperature over Egypt. Atmos Sci Lett 6:176–182

Heltshe JF, Forrester NE (1985) Statistical evaluation of the jackknife estimate of diversity when using quadrat samples. Ecology 66:107–111

Holtslag AAM, de Bruijn EIF, Pan HL (1990) A high resolution air mass transformation model for short-range weather forecasting. Mon Weather Rev 118:1561–1575

Houze RA, James SN, Medina S (2001) Radar observations of precipitation and airflow on the Mediterranean side of the Alps: Autumn 1998 and 1999. Q J Roy Meteorol Soc 127:2537–2558

Jacob D, Podzun R (1997) Sensitivity Studies with the Regional Climate Model REMO. Meteorol Atmos Phys 63:119–129

James CN, Houze RA (2005) Modification of precipitation by coastal orography in storms crossing Northern California. Mon Weather Rev 133:3110–3131

Kahana R, Ziv B, Enzel Y, Dayan U (2002) Synoptic climatology of major floods in the Negev desert, Israel. Int J Climatol 22:867–882

Kalnay E, Kanamitsu M, Kistler R et al (1996) The NCEP/NCAR 40-Year Reanalysis Project. Bull Am Meteorol Soc 77:437–471

Khain AP, Sednev I (1996) Simulation of precipitation formation in the Eastern Mediterranean coastal zone using a spectral microphysics cloud ensemble model. Atmos Res 43:77–110

Khain AP, Rosenfeld D, Sednev IL (1993) Coastal effects in the Eastern Mediterranean as seen from experiments using a cloud ensemble model with a detailed description of warm and ice microphysical processes. Atmos Res 30:295–319

Khain AP, Sednev IL, Khvorostyanov VI (1996) Simulation of deep convection-breeze interaction in the Eastern Mediterranean using a cloud ensemble model with an explicit description of warm and ice microphysical processes. J Climate 9:3298–3316

Kiehl JT, Hack JJ, Bonan GB, Boville BA, Briegleb BP, Williamson DL, Rasch PJ (1996) Description of the NCAR Community Climate Model (CCM3), Tech Rep TN-420+STR, NCAR, Boulder, 152 pp

Köppen W, Geiger R (1936) Das geographische system der klimate. In: Köppen W, Geiger R (eds) Handbuch der klimatologie. Bd 1, Teil C. Verlag Gebrüder Bornträger, Berlin, 44 p

Krichak SO (2008) Regional climate model simulation of present-day regional climate over European part of Russia with RegCM3. Russian Meteorology and Hydrology, 1, 31-41 (Allerton Press, Inc), In Russian. English version is available online from http://www.springerlink.com/content/120692/?p=b1704f828c724ceebc32cbb88bc4cd15&pi=0

Krichak SO, Alpert P, Krishnamurti TN (1997) Interaction of topography, tropospheric flow: a possible generator for the Red Sea Trough? Meteorol Atmos Phys 63:149–158

Krichak SO, Tsidulko M, Alpert P (2000) Monthly synoptic patterns with wet/dry conditions in the eastern Mediterranean. Theor Appl Climatol 65:215–229

Krichak SO, Alpert P, Bassat K, Kunin P (2007) The surface climatology of the eastern Mediterranean region obtained in a three-member ensemble climate change simulation experiment. Adv Geosci 12:67–80. www.adv-geosci.net/12/67/2007

Krichak SO, Alpert P, Kunin P (2009) Projections of climate change over non-boreal east Europe during first half of twenty-first century according to results of a transient RCM experiment. In: Groisman PYa, Ivanov SV (eds) Regional aspects of climate-terrestrial-hydrologic interactions in non-boreal eastern Europe, Springer, NATO Science for Peace and Security Series, Series C: Environmental Security, pp 55–62

Levin N, Saaroni H (1999) Fire weather in Israel—synoptic climatological analysis. GeoJournal 47:523–538

Levin Z, Breitgand J, Shtivelman D (2004) Precipitation over the sea in the coastal area of Israel: a possible new source of water. In: 14th international conference on clouds and precipitation, 20 July, pp 1228–1231

Lionello P, Bhend J, Buzzi A, Della-Marta PM, Krichak SO, Jansa A, Maheras P, Sanna A, Trigo IF, Trigo R (2006) Cyclones in the Mediterranean region: climatology and effects on the environment, pp 325–372. In: Lionello P, Malanotte-Rizzoli P, Boscolo R (eds) Mediterranean climate variability, vol 4. Amsterdam, Elsevier

Mitchell TD, Carter TR, Jones PD, Hulme M, New M (2004) A comprehensive set of high-resolution grids of monthly climate for Europe and the globe: the observed record (1901–2000) and 16 scenarios (2001–2100), Tyndall Centre Working Paper No. 55. Tyndall Centre for Climate Change Research. University of East Anglia, Norwich

New M, Hulme M, Jones P (2000) Representing twentieth-century space-time climate variability. Part II: Development of 1901–1996 monthly grids of terrestrial surface climate. J Clim 13(13):2217–2238

Pal JS, Giorgi F, Bi X, Elguindi N et al (2007) The ICTP RegCM3 and RegCNET: regional climate modeling for the developing world. Bull Am Meteorol Soc 88(9):1395–1409

Rodwell MJ, Hoskins B (1996) Monsoons and the dynamic of deserts. Q J Roy Meteorol Soc 122:1385–1404

Saaroni H, Bitan A, Alpert P, Ziv B (1996) Continental polar outbreaks into the eastern Mediterranean. Int J Climatol 16:1175–1191

Saaroni H, Ziv B, Bitan A, Alpert P (1998) Easterly windstorms over Israel. Theor Appl Climatol 59:61–77

Seth A, Giorgi F (1998) The effects of domain choice on summer precipitation simulation and sensitivity in a regional climate model. J Clim 11:2698–2712

Stenchikov G, Hamilton K, Stouffer RJ, Robock A, Ramaswamy V, Santer B, Graf H-F (2006) Arctic oscillation response to volcanic eruptions in the IPCC AR4 climate models. J Geophys Res 111:D07107. doi:10.1029/2005JD006286

Takle ES, Roads J, Rockel B, et al (2007) Transferability intercomparison: an opportunity for new insight on the global water cycle and energy budget. Bull Am Meteorol Soc, March, pp 375–384

Trigo IF, Davies TD, Bigg GR (1999) Objective climatology of cyclones in the Mediterranean Region. J Clim 12:1685–1696

Tsvieli Y, Zangvil A (2005) Synoptic climatological analysis of wet and dry Red Sea troughs over Israel. Int J Climatol 25:1997–2015

Vannitsem S, Chome F (2005) One-way nested regional climate simulations and domain size. J Clim 18:229–233

Yatagai A, Alpert P, Xie P (2008) Development of a daily gridded precipitation data set for the Middle East. Adv Geosci 12:1–6

Zeng X, Zhao M, Dickinson RE (1998) Intercomparison of bulk aerodynamic algorithms for the computation of sea surface fluxes using TOGA COARE and TAO data. J Clim 11:2628–2644

Ziv B, Saaroni H, Alpert P (2004) The factors governing the summer regime of the eastern Mediterranean. Int J Climatol 24:1859–1871

Ziv B, Dayan U, Sharon D (2005) A mid-winter, tropical extreme flood-producing storm in southern Israel: synoptic scale analysis. Meteorol Atmos Phys 88:1–2–53–63

Ziv B, Dayan U, Kushnir Y, Roth C, Enzel Y (2006) Regional ana global atmospheric patterns governing rainfall in the southern Levant. Int J Climatol 26:55–73